Chemical Physics 579 (2024) 112200

Contents lists available at ScienceDirect

Chemical Physics

journal homepage: www.elsevier.com/locate/chemphys

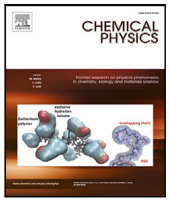

Proposing a plausible molecular structure for Ice XI: A coupled study using Rietveld refinement and Density Functional Theory

Christina M.B. Biggs *, Darren L. Oatley-Radcliffe

Energy Safety Research Institute, College of Engineering, Swansea University Bay Campus, Fabian Way, Swansea, Wales SA1 8EN, United Kingdom

ARTICLE INFO

Keywords:
Ice XI
Rietveld refinement
Density functional theory

ABSTRACT

A plausible molecular structure for fully ordered Ice XI is proposed. A range of structures were generated by varying the lattice parameters along the trajectory of the observed Ice Ih/Ice XI phase transition and recording the energy-minimised Density Functional Theory structure (using the Perdew–Wang 1991 functional) for each set of lattice parameters. These proposed structures were then fitted to the neutron data using GSAS-II to extract the goodness-of-fit. It is shown that the Rietveld refinement was insensitive to the OH_1 bond length and the HO_2H bond angle. The refinement with the lowest value of Rw^2=6.038% gave OH bond lengths of 0.997(7)Å, 0.999(2)Å, 0.997(5)Å, HOH bond angles of 107.5° and 106.0°, and OH...O hydrogen bond lengths of 1.77(4),1.75(2) and 1.75(1)Å. It is therefore apparent that the two crystallographically distinct water molecules have very similar molecular hydrogen bond parameters, which are close to that predicted by previous CASTEP PW91 DFT modelling.

1. Introduction

Ice XI (Ice-eleven), the low-temperature ordered form of Ice Ih, is known to be orthorhombic with symmetry $Cmc2_1$ [1–5]. It is currently synthesised by doping water with potassium hydroxide (KOH) at a low concentration, as the proton vacancies generated by the doping facilitate the reorientation of the water molecules to give the ordered low-temperature structure of Ice XI.

Ice XI is of interest because it represents a lower energy state than the disordered ordinary Ice Ih, and because small domains of Ice XI have been observed in liquid water [6]. It has also been observed to form under UV conditions [7], leading to speculation that Ice XI could be involved in the formation of planets, and thereby to efforts to predict the infrared spectral signature of Ice XI for identification in space ([8–12], and [13]). The only previous refinement of Ice XI neutron diffraction data was performed by [1] which gave an unrealistic HOH angle of 114°. A range of methods of predicting the structure and its phase transition have been used, principally using Density Functional Theory (notably [5,11,14,15]). Although the OH bond-stretching modes seen in the Raman and FTIR spectra appear to be relatively insensitive to the Ice XI structural ordering, the librational modes of Ice XI, as seen by inelastic neutron scattering [16–18] have been shown to sharpen in Ice XI and have been partially assigned to collective librational modes by [19,20]. Clearly a more precise determination of the structure of Ice XI would be welcome in progressing this work.

Neutron diffraction can be used to locate the position of hydrogen atoms, provided the hydrogen is replaced by deuterium, i.e. using D_2O doped with KOD for neutron experiments. Undoped ice shows partial transformation when annealing at low temperature for several months [3]. When slowly heating the Ice XI through the transition temperature of 72 K, the lattice parameters converge onto that for Ice Ih in a second-order phase transition [2,3]. When the ratio between the lattice parameters c and a are plotted as a function of temperature across the phase transition, the data from [2,3] match [3]. Full conversion from Ice Ih to Ice XI has not yet been achieved, except possibly under UV irradiation by [7], and this partial conversion (and therefore the usual observation that Ice XI always occurs with untransformed Ice Ih) is thought to be due to the inherent strain associated with the breaking of symmetry from hexagonal Ice Ih to orthorhombic Ice XI. This also produces anisotropic broadening of the diffraction peaks [2]. This is the main reason why accurate structural data for Ice XI has not yet been determined.

The symmetry of Ice XI has been established to be orthorhombic with space group $Cmc2_1$ [1] and confirmed to be ferroelectric by [21] with a shift along the b-axis in adjacent ice layers [22]. The ordering scheme is shown in Fig. 1, with two types of water molecule: O1 having one OH bond (OD bond in deuterated ice) pointing along the c-axis (giving rise to ferroelectric ordering) and the other OH (or OD) bond in the plane parallel to the b-axis, and O2 having OH (or OD) bonds

* Corresponding author.
E-mail addresses: cmbbiggs@gmail.com (C.M.B. Biggs), d.l.oatley@swansea.ac.uk (D.L. Oatley-Radcliffe).

https://doi.org/10.1016/j.chemphys.2024.112200
Received 18 September 2023; Received in revised form 10 November 2023; Accepted 16 January 2024
Available online 18 January 2024

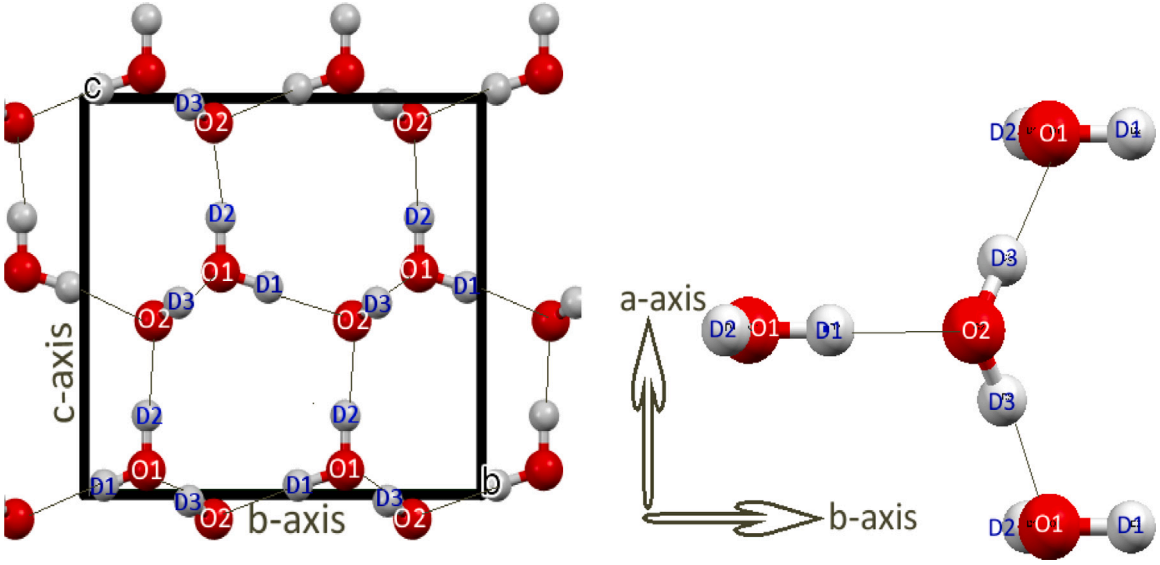

Fig. 1. Structure of Ice XI, viewed (left) down *a*-axis, and (right) down *c*-axis. On right, origin of axes offset for clarity.

Table 1
Lattice parameters used in each of the CASTEP and GSAS-II fitting. D_2O ice samples and CASTEP models throughout.

Model	a (Å)	b (Å)	c (Å)
Ice Ih pure (10 K) [23]	4.49728(1)	7.78951(2)	7.32403(1)
Ice Ih pure (5 K) [2]	4.4974	7.789	7.3236
Ice Ih (5 K) mixed with Ice XI [2]	4.499	7.792	7.311
Ice Ih (10 K) mixed with Ice XI (this study, Rietveld refinement)	4.499(3)	7.791(3)	7.311(fix)
Ice XI [3] (in Supplementary Material)	4.49771(1)	No data	7.31922(3)
Ice XI Rietveld [1]	4.5019	7.7978	7.328
Ice XI (5 K) [2]	4.465	7.858	7.292
Ice XI CASTEP (PW91) optimised [5]	4.383	7.617	7.207
Ice XI Rietveld, this study, free fit	4.4717(3)	7.8487(6)	7.29223(2)
Ice XI Rietveld, "best in class" *c* fixed to [2]	4.4749(3)	7.8452(6)	7.292(fix)
Ice XI CASTEP (PW91) this study	4.4749(fix)	7.8452(fix)	7.292(fix)

symmetrically positioned about a mirror plane parallel to the b- and c-axes and pointing alternately along +b and −b in adjacent layers (hence antiferroelectric with respect to the *b*-axis although ferroelectric with respect to the *c* axis). For accuracy, the diagrams and data tables in this paper refer to deuterated ice, but for clarity of discussion on ice in general, the text refers to hydrogen rather than deuterium.

The effect of the ordering is to shorten the *c*-lattice parameter, shorten *a* and lengthen *b*, as summarised in Table 1. In Ice Ih, the hexagonal symmetry gives three equivalent directions (at 120°) for *a* in the plane perpendicular to *c*. When Ice XI is formed, the breaking of symmetry to orthorhombic can occur along any of these three directions, which means that domains of Ice XI form in three orientations, and where these domains meet there is considerable mismatch in lattice parameter, causing lattice strain. This does not occur along the *c*-axis as the Ice XI and Ice Ih *c*-axes are in the same direction.

When the first high-resolution powder diffraction study was undertaken in 1995 [2], the diffraction peaks were found to be anisotropically broadened, and at the time the existing GSAS software was not able to model this peak broadening and satisfactorily extract a molecular structure. Since then, the GSAS-II software has been developed which can model anisotropic peak broadening [24], and the results of the analysis using GSAS-II are presented in this paper, together with a Density Functional Theory (DFT) simulation using CASTEP with the PW91 functional, as used by [4,5] for Ice XI simulations.

The focus of this paper is two-fold: modelling the Ice XI anisotropic strain broadening in order to extract a full Rietveld refinement to determine the precise molecular geometry of Ice XI: including HOH bond angles, OH bond lengths, H…O hydrogen bond distances and O…H–O hydrogen bond angles; and carrying out DFT calculations to compare the calculated geometry with the Rietveld refinement. Given that the HOH bond angle in Ice Ih is known to be less than the tetrahedral OOO bond angle of 109° [25], it is interesting to view the Ice XI structure as a test-bed for evaluating the effect of stress on the water molecule and how the stiffness of the HOH angle and the OHO hydrogen bond angles balance each other. In turn, this could help in selecting the most appropriate molecular dynamics model for ice, in particular finding the stiffness of the hydrogen bond which is so important in giving Ice Ih its low density relative to liquid water.

2. Experimental

2.1. Neutron diffraction study

2.1.1. Neutron data collection

The diffraction data for this study was collected from the High Resolution Powder Diffractometer (HRPD) at the ISIS neutron spallation source at the Rutherford Appleton Laboratory, Didcot, UK. The experiment was carried out by Dominic Fortes in the course of his investigation into the temperature-dependence of the lattice parameters and peak broadening of high-resolution neutron diffraction data of Ice XI through the phase transition from Ice Ih, reported in [3].

The sample was D_2O ice doped with 2 mM of KOD (40 wt% in D_2O, 98 atom% D, Sigma 176 761) in pure D_2O (99.96 atom% D, Sigma 151 890). This liquid was pipetted into liquid nitrogen and the ice ground to a fine powder and the sample annealed for 15 h at 70 K, just below the phase transition temperature of 72 K, before cooling to 10 K for the high-resolution run analysed in this present study.

The previous report of this experiment [3] focused on the variation of lattice parameters with temperature across the Ice XI/Ice Ih phase transition at 72 K of a range of ice samples, including pure D_2O ice which was annealed for several months and showed partial transformation, as shown by the change in the ratio between a and c across the phase transition. The KOD-doped Ice XI used for our Rietveld refinement showed a more complete transformation with the ratio c/a similar to that found by [2] for a different KOD-doped Ice XI sample.

This present study uses only the 10 K, high resolution run of the KOD-doped ice, referred to in the Supplementary Material of [3] as Series 7, and is the first attempt to quantify the anisotropic strain broadening of Ice XI in order to extract accurate molecular co-ordinates of Ice XI.

2.1.2. Lattice parameters

The lattice parameters a, b and c of Ice XI for previous studies are reported in Table 1, together with those measured in the present study. To facilitate comparison, Table 1 gives a value of b for Ice Ih which is equal to $a\sqrt{3}$.

It can be seen that there is some variability in lattice parameters which is due to differences in sample preparation and possibly in diffractometer calibration.

Unlike an X-ray spectrometer which uses a constant wavelength and a range of diffraction angles, a neutron spallation source such as ISIS uses short pulses of neutrons with a range of velocities (and therefore wavelengths) but a fixed angle. The time-of-flight of the neutrons is converted to Q, the change of momentum, and from there to d-spacing, which then can be used to index the diffraction peaks.

Two detector banks were used, the highest resolution being Bank 1 at an average 2θ of 168.33° and a low-resolution Bank 2 at an average 2θ of 90°, and both banks were used in the Rietveld refinement.

The complete neutron diffraction patterns from Bank 1 and Bank 2 are shown in Fig. 2. The range in d-values is high and therefore provides information to a high spatial precision, and the two banks overlap in d-spacing. A more detailed view, seen in Figs. 4, 5, and 6, shows that the much broader instrumental peak width of the Bank 2 diffraction peaks serve to hide the detail of the peak splitting and anisotropic peak broadening in Ice XI. This in fact proved to be a valuable check on the Rietveld fit to the peak intensities (from which the ice structure is calculated) when fitting the high-resolution Bank 1 peaks proved difficult.

Calibration of a neutron diffractometer relies not just on focusing the diffractometer banks, but also using accurate time-of-flight data for the neutrons. The programme GSAS-II [24] used to carry out a Rietveld analysis of the data, has several parameters that can be refined, notably dif-C and dif-A, as described in [23], which are normally refined to a silicon standard, and result in a value of dif-C that is recommended by the instrument scientist for subsequent refinement.

For the present study, no silicon standard was made available, and therefore the default value of dif-C was used. A free fit using this value of dif-C resulted in the lattice parameters given in Table 1, which is similar to that obtained by [2] for a different sample of Ice XI.

However, the fact that the sample was composed of a mixture of Ice XI and untransformed Ice Ih, with overlapping peaks, meant that the freely-refined c-lattice parameters of Ice XI and Ice Ih became more similar to each other, as seen in Table 1, and resulted in a poor fit to the {004} peak in Fig. 3. The structural refinement for these converged lattice parameters gave implausible molecular geometry, notably very large (110°) or small (102°) HOH angles. To prevent this, the c-lattice parameters for Ice XI and the untransformed Ice Ih were fixed to the values found by [2], as shown in Table 1, while the a and b lattice parameters allowed to vary freely.

It is possible therefore that the different value obtained by [3] for the same data was due to a more accurate calibration, or because the value used was taken from a fit over the merged peaks.

This still gave a small discrepancy in the position of the {131} peak relative to that calculated from the lattice parameters (see Fig. 5), consistent with that observed by [1]. The relative intensity of the {004} peaks in Figs. 3 and 4 are also anomalous, as also noted by [26].

2.1.3. Anisotropic peak broadening

It can be seen from Fig. 4 that the peak widths of the {004} peaks are much narrower than the {22l} and {04l} peaks. This has been noted before by [2,27], and is due to the hexagonal symmetry of Ice Ih having three possible orientations for b (at 120° to each other) when breaking symmetry to Ice XI, as explained in the Introduction.

As domains of Ice XI will form in Ice Ih in these three orientations, due to the mismatch in the new a and b lattice parameters, this will set up lattice strain. An alternative interpretation, used by [1,3], is that the different domains forming at 120° to each other will impinge on each other and prevent growth, and the peak broadening is due to small domain sizes.

On the other hand, the {004} peaks do not broaden because the Ice XI domains formed are parallel to each other, causing less lattice strain. This can be seen in Fig. 4.

To deal with this, the programme GSAS-II [24] now has an anisotropic strain broadening function. This uses the following formula, specific to the orthorhombic symmetry of Ice XI [28]:

$$\sigma^2(M_{hkl}) = S_{400}h^4 + S_{040}k^4 + S_{004}l^4 + 3(S_{220}h^2k^2 + S_{202}h^2l^2 + S_{022}k^2l^2) \quad (1)$$

where $M_{hkl} = 1/d^2$ (where d is the d-spacing of the {hkl}-indexed peak), σ^2 is the variance in M_{hkl}, and S_{abc} are the strain-broadening parameters that can be varied in GSAS-II. There is a simpler form for the hexagonal Ice Ih:

$$\sigma^2(M_{hkl}) = S_{400}h^4 + S_{004}l^4 + 3S_{202}h^2l^2 \quad (2)$$

and the optimised values of S_{abc} are given in Table 2.

The peak shape of the {131} peak seen in Fig. 5 and later in Fig. 10, being the only single peak to only occur in Ice XI and not Ice Ih, was very close to pure Lorentzian and therefore the peak shape for the strain broadening was set to pure Lorentzian. The peak shape of the {004} peaks, also observed by [2], was more Gaussian (see Fig. 3), but this was because the {00l} peaks showed no strain broadening relative to the default Gaussian peak shape on Bank 1. Thus the anisotropic strain parameter along this axis (S_{004}) was taken to be unitary (a value of 1000 in the GSAS program), and the cross terms including the {00l} (ie S_{202} and S_{022}) were set to zero, as recorded in Table 2.

As this is the first time that an anisotropic strain model has been used for Ice XI, it is interesting to note the negative value of the refined cross-component S_{220} given in Table 2 (from Eq. (1)). This is due to the fact that the {h0l } peaks and the {0kl} peaks are very broad (see Figs. 4 and 5) whereas the {hhl} and {h3hl} peaks are much narrower. This is proposed to be due to the fact that when transforming from Ice Ih to Ice XI, the a lattice parameter decreases and the b lattice parameter increases (see Table 1). This means that oblique lattice planes such as {110} and {130} would have less variability than the {100} and {010} peaks and therefore have narrower peaks.

The narrowness of the {130} peak relative to the {110} peak in Fig. 10, and the sharpness of the {062} and {260} peaks in Fig. 6 could be evidence that this peak-narrowing effect is the most pronounced in the {h3h0} direction. However, the value of S_{220} that gives the best fit to the {hhk} peaks does not simultaneously fit the {13k} peaks. This could be a limitation of the [28] model itself. These peaks are also close in position to aluminium, which was the material used for the sample container. In any case, as the intensity of the {260} and {062} peaks were low compared to the other peaks, it was decided to ignore this for the purposes of determining the structure of Ice XI.

Developers of Rietveld refinement programs may be interested in exploring this further. However, the Bank 2 results for each of these peaks showed that the combined integrated intensities fitted well to the Rietveld model, so it was therefore decided that the [28] model was sufficient for the purpose of determining a plausible crystal structure for Ice XI.

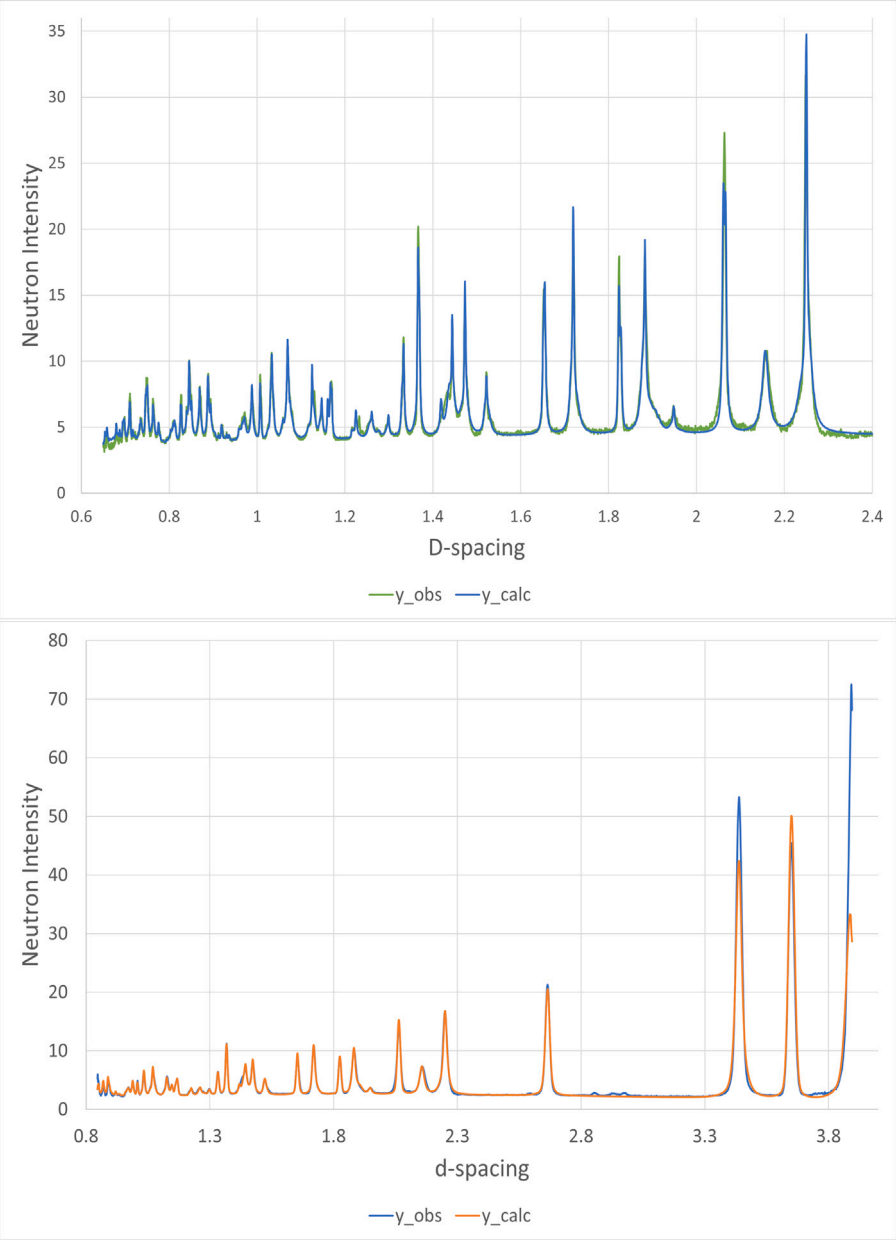

Fig. 2. Complete neutron diffraction pattern for Bank 1 (top) and Bank 2 (bottom).

Table 2
Table showing final values of anisotropic peak parameters,according to model proposed by [28], shown in Eq. (1). Accuracy to two significant figures.

Phase	Strain parameter	Rw = 6.111%
Ice XI	S_{400}	260,000
	S_{040}	41,000
	S_{004}	1000 (=unitary)
	S_{220}	−39,000
	S_{202}	0.0
	S_{022}	0.0
Ice Ih	S_{400}	8700
	S_{004}	1000
	S_{202}	0.0

2.1.4. Particle size versus strain broadening

Although particle size broadening (which also has an anisotropic functionality) was modelled, this led to no improvement in the fit, either in isolation or when modelled at the same time as the anisotropic strain broadening. The angle-dependence of the two are different, with particle size broadening giving Δd proportional to d^2 and strain broadening giving Δd proportional to d [29]. Fig. 7 compares a low and high range of d when fitting to particle size broadening only, showing that when the low-d region is fitting peak widths well, the high-d peaks do not fit the particle-size model.

Moreover, particle size broadening is also inconsistent with the observation that the {hh0} and {h 3h 0} peaks were narrower than the {h00} and {0h0} peaks, as the generalised anisotropic particle-size model, in the version of GSAS-II used, was an ellipsoid in shape, but the strain broadening function have negative cross-terms. For the equivalent crystallite with dimensions Δa and Δb, the oblique term will be intermediate between the two, at least for the ellipsoidal model available in GSAS-II.

This verdict of strain broadening rather than particle size broadening is in disagreement with the study carried out on the same data by [3] who reported that there was no anisotropic strain broadening but that all the broadening was due to particle size broadening, and also

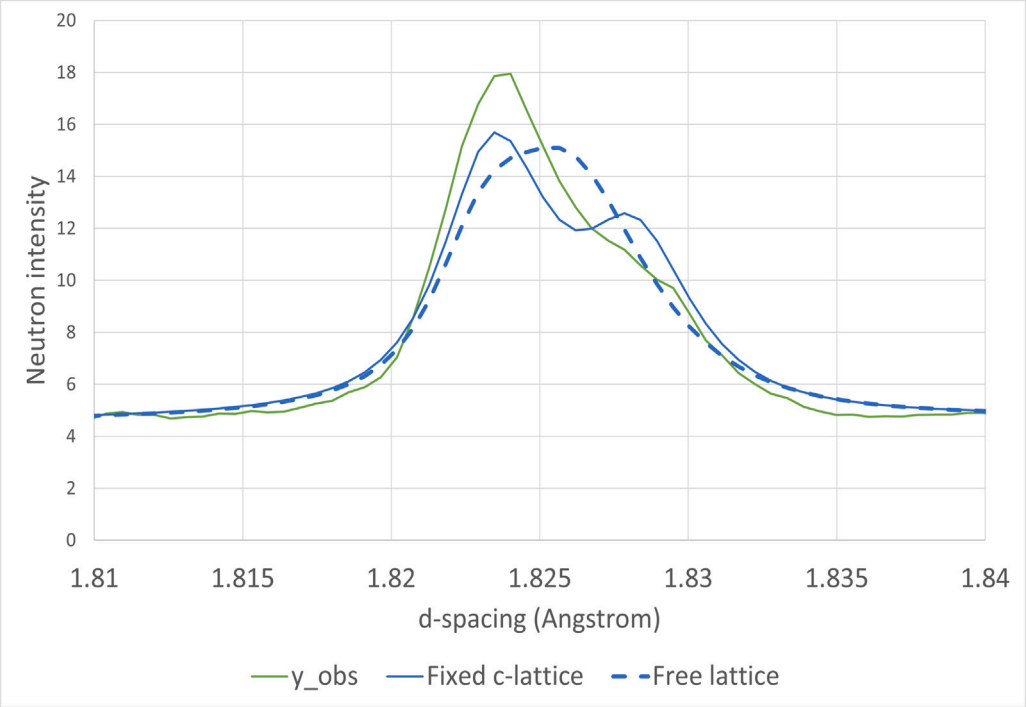

Fig. 3. Neutron diffraction {004} peak, showing inadequacy of allowing free fitting of lattice parameters.

to [1] who interpreted the Lorentzian shape as due to domain sizes of 40 Å. However, neither [3] nor [1] had reported the d-dependence of the broadening nor attempted a fit for anisotropic peak broadening.

In any case, for the purposes of determining the molecular structure of Ice XI, the overriding need is to fit the peaks to give the correct integrated intensities for the structural model, so the precise method of fitting is less important. Bank 2, where the intrinsic peak profiles are much broader so that the Ice XI and Ice Ih peaks are merged, gives a useful check on the fitted total peak intensities of the merged peaks.

2.1.5. Rietveld refinement of atomic co-ordinates

The starting atomic co-ordinates of Ice XI were taken from those calculated using CASTEP by [5]. Once satisfactory lattice parameters (with c fixed as described in Section 2.1.2)and peak shapes were obtained (as reported in Tables 1 and 2), all atomic co-ordinates of Ice XI and isotropic displacement parameters U_{iso} were refined freely with no rigid-body constraints. The molecular co-ordinates of Ice Ih were fixed to those quoted in [30].

Initially, negative U_{iso} isotropic displacement parameters were obtained for the oxygen atoms in Ice XI and Ice Ih, but this was resolved by fitting a sample absorption parameter, constrained to be the same for each of the three detector banks, and also constraining the two oxygen atoms in Ice XI to have the same U_{iso} as the Ice Ih oxygen.

The standard deviation in atomic co-ordinates (seen as brackets in Table 3) was calculated by the GSAS-II program. GSAS-II also gave the uncertainty in the HOH bond angle and bond lengths.

The final Rietveld refinement was also used to test a large range of atomic co-ordinates, both from the literature and from calculations using Density Functional Theory below, by fixing the atomic co-ordinates to the test values, keeping the GSAS-II refined lattice parameters, and also keeping the anisotropic strain parameters constant at the values in Table 2. The R_w^2 output parameter was used throughout to measure goodness-of-fit. The results of these tests are summarised in Fig. 9.

2.2. Density functional theory calculations

The programme used for DFT modelling used was CASTEP [31], which uses plane waves in a unit cell with periodic boundary conditions. The Perdew–Wang 1991 functional [32] was used, as this was used by [4] for correctly predicting the $Cmc2_1$ symmetry of Ice XI and also by [5] in evaluating the fully relaxed DFT prediction of the atomic co-ordinates of Ice XI. The Koelling–Harman correction scheme was used as default [33]. The Broyden, Fletcher, Goldfarb, and Shanno, or BFGS algorithm [34] was used for the geometry optimisation, and the starting Ice XI co-ordinates taken from [5]. The relative atomic mass of the hydrogen atoms were set to 2.0 for equivalence with deuterated Ice XI.

As well as generating the energy-minimised molecular structure for the measured Rietveld-refined "best in class" lattice parameters of Ice XI from Table 1, reported in Table 6, CASTEP was used to generate a set of candidate structures by varying the cell parameters along a single trajectory from those of pure ice along the phase transition to Ice XI, and extrapolating the lattice parameters beyond those measured for Ice XI. Each energy-minimised set of atomic co-ordinates from CASTEP was tested in the Rietveld refinement (but unavoidably using the GSAS-II refined lattice parameters rather than the deliberately-varied CASTEP lattice parameters) to extract the goodness-of-fit to the neutron data.

Each of these CASTEP energy-minimised structures, as well as the Rietveld refinement using the freely fitted atomic co-ordinates, was analysed to extract the molecular parameters such as HOH bond angle, OH bond length, OH...O hydrogen bond length and OHO hydrogen bond angle, and other deviations from the Ice Ih structure such as wag, rock, b-shift and pucker, as defined in Fig. 8. The results of this fitting process are shown in Fig. 9, with the numerical value of the optimal parameters for the "best in class" free Rietveld fit given in Table 3 and the results of the CASTEP energy minimised structure for the same lattice parameters as the free Rietveld fit given in Table 4, with a comparative summary in Table 6.

When testing CASTEP models where the lattice parameters differed from those used in the Rietveld refinement, the molecular parameters (HOH, OH, wag, rock and pucker) were initially extracted using the original lattice parameters and then used to generate the input structure to the Rietveld refinement to avoid distorting the water molecules, but these gave very similar fits to using the fractional coordinates direct, so are not elaborated on here.

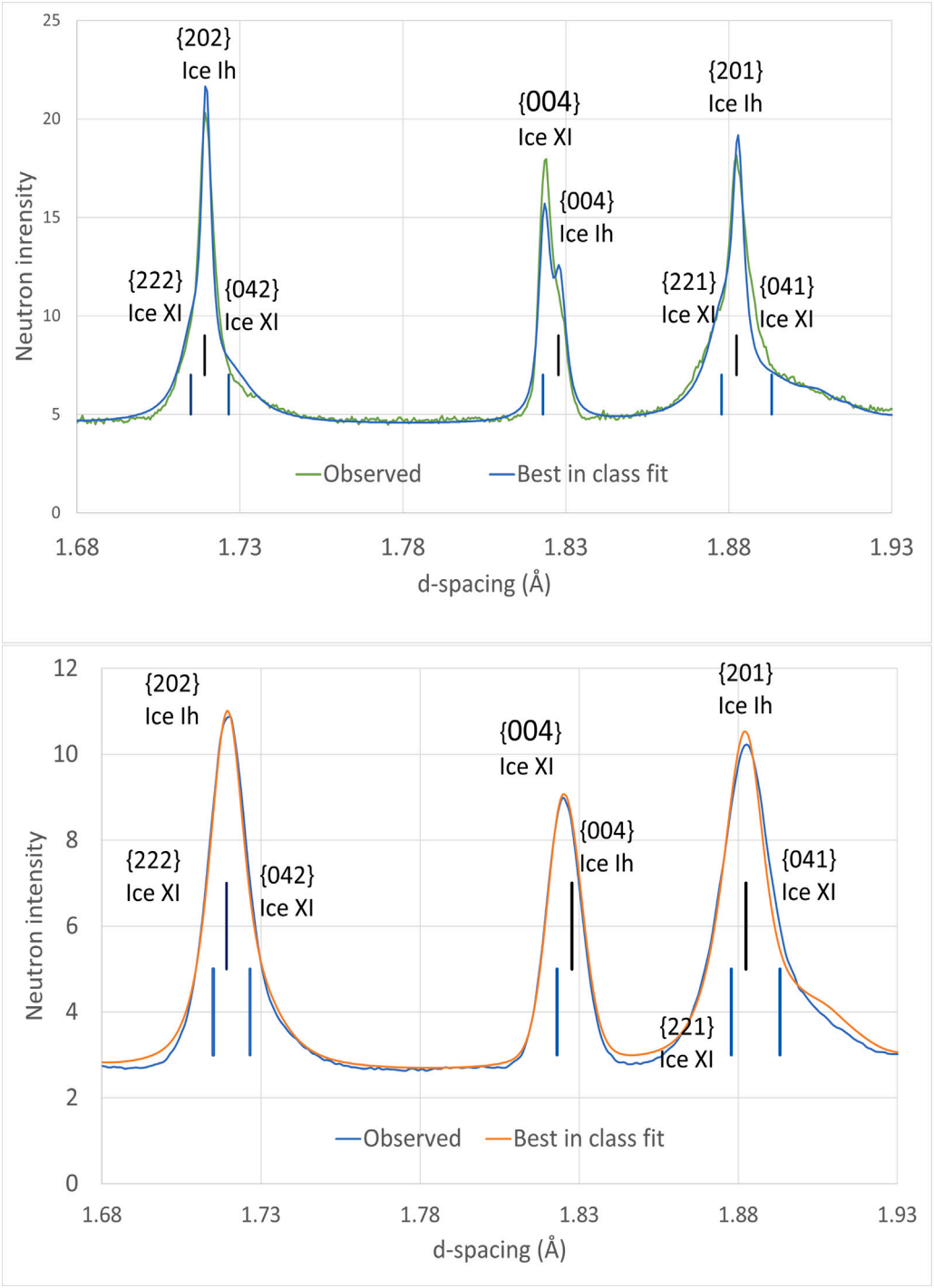

Fig. 4. Neutron diffraction pattern near {004} peak, showing anisotropy in peak profiles: Bank 1 (top, high resolution) and Bank 2 (bottom, low resolution). The different indexing of equivalent Ice XI and Ice Ih peaks is due to the hexagonal symmetry of Ice Ih and the orthorhombic symmetry of Ice XI.

3. Results

3.1. Rietveld refinement

3.1.1. Lattice parameters

The refined lattice parameters are reported in Table 1 alongside those obtained in previous studies, including D_2O Ice Ih. The discrepancy between [3] parameters and those measured in the current study (which relate to the same neutron data) could be due to a more accurate calibration or simply be due to the [3] parameters being measured as the centre of the Ice XI/Ice Ih combination peaks, as this gives values intermediate between Ice XI and Ice Ih.

3.1.2. Peak shape

As noted before and seen in Figs. 3 and 4, the {004} peak is shown to be split into two Gaussian peaks, with the peak corresponding to Ice XI having the greater intensity despite the phase fraction of Ice XI being smaller than that of Ice Ih. This anomaly in relative intensity of the {004} peaks was not fully reproduced by the Rietveld fit (as also

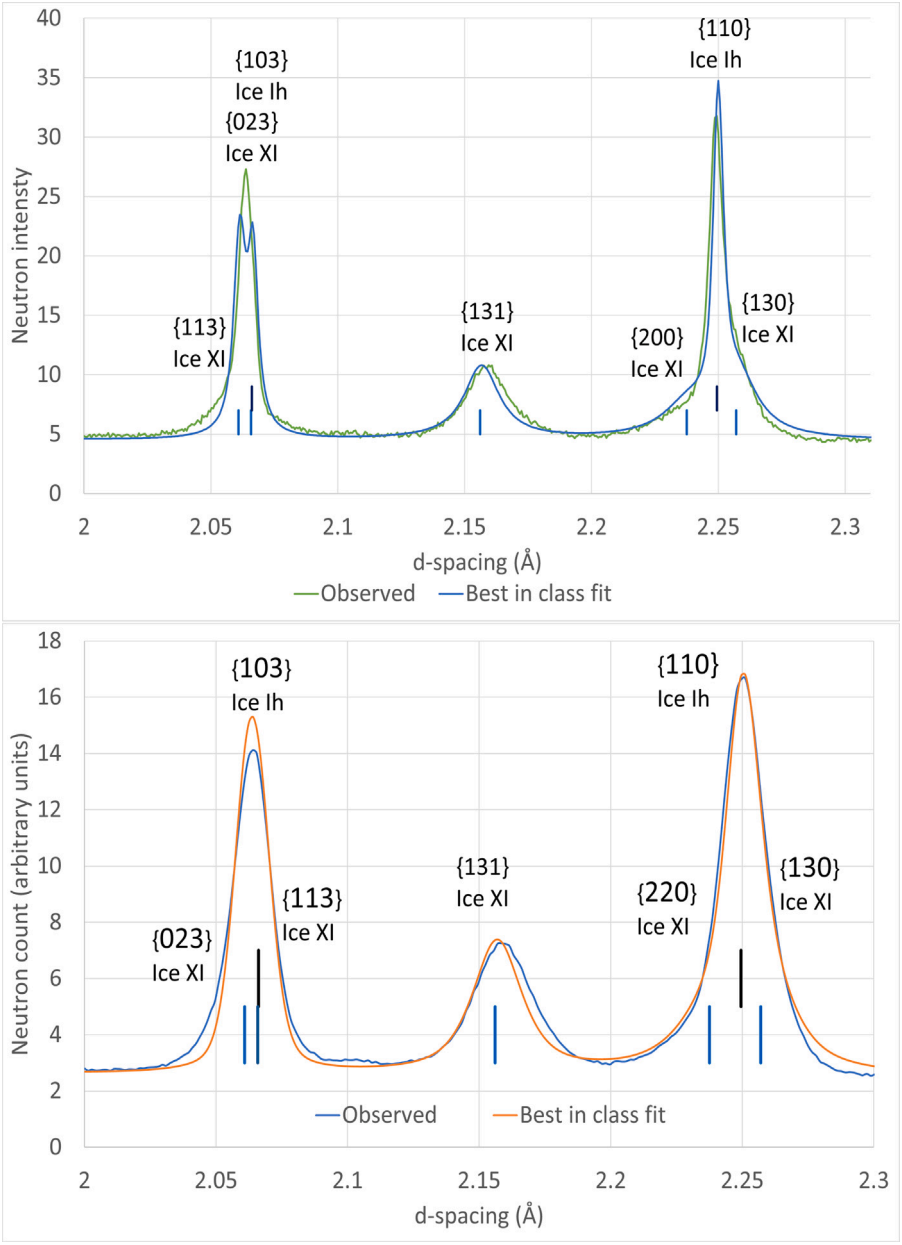

Fig. 5. Neutron diffraction pattern for {131} peak for Bank 1 (top, high resolution) and Bank 2 (bottom, low resolution with larger peak widths), showing difference in intrinsic peak widths. The different indexing of equivalent Ice XI and Ice Ih peaks is due to the hexagonal symmetry of Ice Ih and the orthorhombic symmetry of Ice XI.

shown in Fig. 3), and has been previously observed by [27]. Attempts were made to improve the relative intensities, which simply worsened the fit elsewhere, so this remains unaccounted for and has been ignored for the structural determination.

As already noted by [2], the {131} peak, being the only non-overlapping single diffraction peak attributable to Ice XI, has a Lorentzian shape rather than a Gaussian shape, which is compatible with strain broadening. On the other hand, the {004} peaks were much narrower than the {131} peak, and had more of a Gaussian shape, with a width close to that of the intrinsic peak function for HRPD, and was fitted to value of 1000 (indicating no strain broadening in the c direction) in Table 2 for the anisotropic strain parameter S_{004}.

The table of final fitted anisotropic strain values is shown in Table 2. The S_{400} and S_{040} parameters gave similar structural fits for values varying by 10% so are quoted to 2 significant figures. The negative value of S_{220} has already been discussed and accounted for in the Experimental section.

3.1.3. Rietveld refinement of molecular structure

As explained in the Experimental section, the starting co-ordinates for Ice XI were those derived from the DFT Perdew–Wang calculations by [5], and the refinement used no rigid-body constraints. The HOH bond angles and OH bond lengths of the various fits, together with the goodness-of-fit R_w^2, are summarised for quick reference in Table 6 and the full "best in class" structure is given in Table 3.

This uncertainty over the correct value of the cell parameters is why it was decided to vary the cell parameters in CASTEP to give a range of candidate molecular structures for input into GSAS-II.

3.2. Density-functional theory (DFT) results using CASTEP

The energy-minimised HOH bond angle and bond lengths of Ice XI from CASTEP are shown in Table 6, which uses the lattice parameters obtained by the Rietveld free refinement with the best goodness of fit. Once the CASTEP co-ordinates were energy-minimised, they were

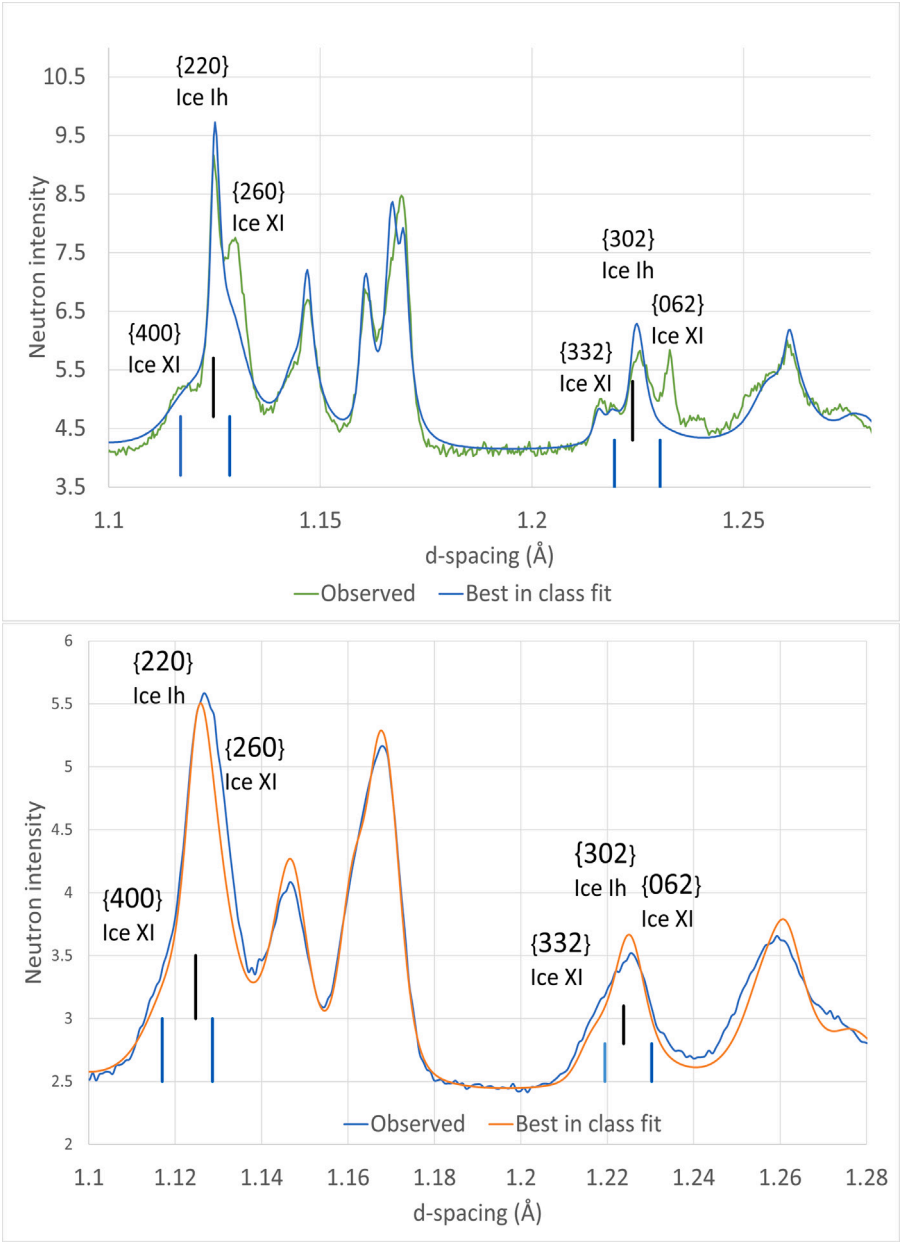

Fig. 6. Neutron diffraction pattern showing inadequacy of anisotropic peak modelling for {260} and {062}, possibly due to limitations in the [28] model. Top, Bank 1, bottom — Bank 2. The different indexing of equivalent Ice XI and Ice Ih peaks is due to the hexagonal symmetry of Ice Ih and the orthorhombic symmetry of Ice XI.

Table 3
Full crystallographic parameters and derived molecular geometry for "best in class" Rietveld free-fit refinement (Rw = 6.111%). As this is from the fit to the deuterated Ice XI, the hydrogens are represented with the D symbol for deuterium.

	a = 4.4749(27) Å	b = 7.8452(5) Å	c = 7.292 Å (fixed)
O1	0.0	0.6556(8)	0.06172
O2	0.5	0.8266(7)	−0.06172
D1	0.0	0.5375(6)	0.0233(6)
D2	0.0	0.6571(5)	0.1987(4)
D3	0.3220(6)	0.7633(4)	−0.0155(5)
D1O1D2	107.5(6)°	D3O2D3	106.0(8)°
O1D1	0.969(7) Å	O1D2	0.999(6) Å
O2D3	0.997(4) Å		
OD1O = 176.3(1)°	OD2O = 176.5(4)°	OD3O = 178.1(3)°	
D1...O = 1.766(2) Å	D2...O = 1.752(1) Å	D3...O = 1.763(3) Å	
OO1O = 112.1(1)°	OO2O = 108.3(4)°		
Pucker = 0.06172(2)*c*	b-shift = 0.00886(2)*b*	W1 rock = −0.096(2)°	W2 wag = −0.25(2)°

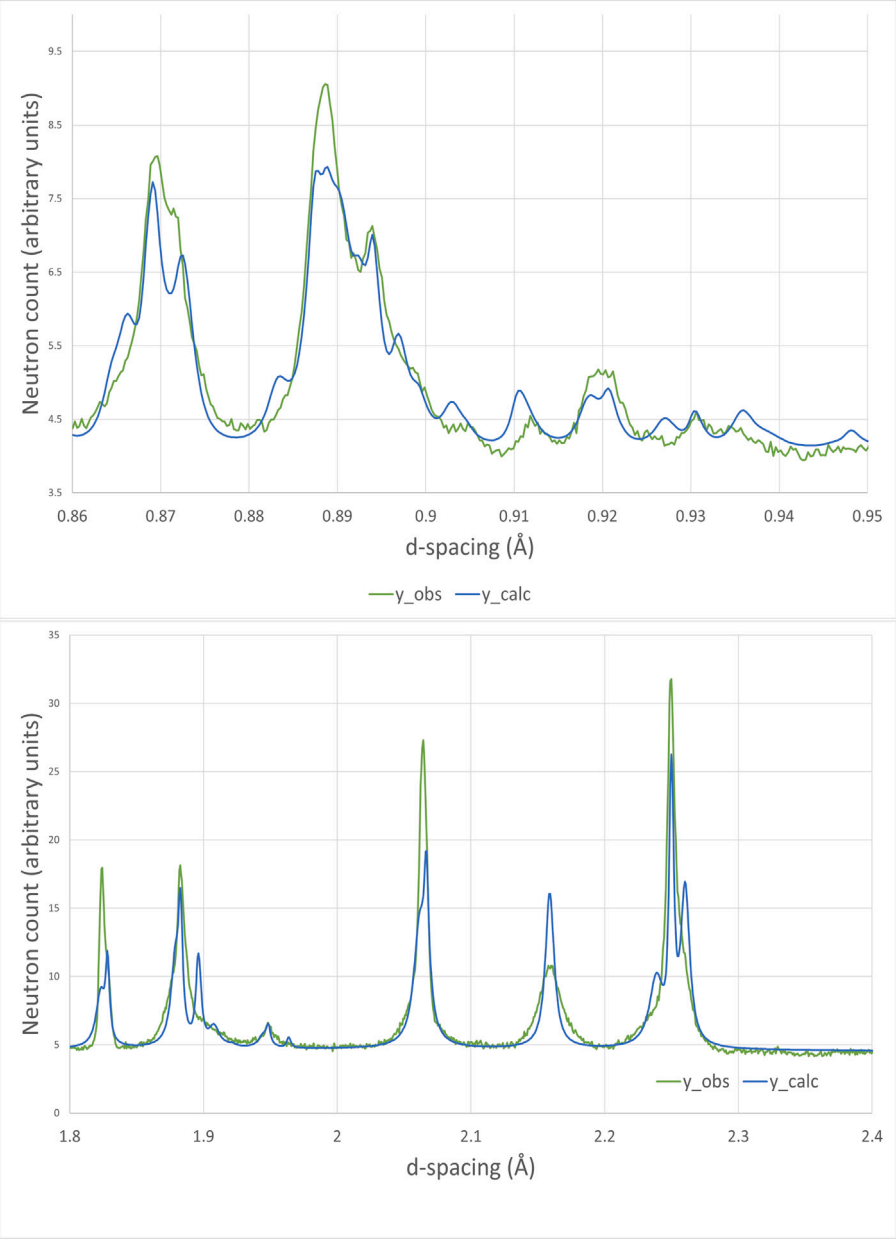

Fig. 7. Neutron diffraction pattern fitted to particle-size broadening only, for low-*d* (showing a good fit to peak widths) and high-*d* (showing a poor fit to the same model).

fixed in the Rietveld refinement, using the Rietveld-refined lattice parameters, to give a goodness of fit of 6.148%. The full co-ordinates and derived molecular parameters are given in Table 4 for comparison with the Rietveld-fitted atomic co-ordinates.

The difference between the [5] CASTEP-derived structure and the present CASTEP study reported in Table 4, and compared in Table 6, is because [5] performed their own cell parameter energy optimisation, which give different cell parameters from the Rietveld fitting.

To determine the uncertainty in the CASTEP measurements, a CASTEP calculation using a slightly different set of lattice parameters, within the uncertainty of the present Rietveld fit (a = 4.47624 Å, b = 7.8448 Å, c = 7.292 Å) was carried out, which when fitted to the Rietveld model gave an R_w^2 of 6.57%. The calculated difference between this and the R_w^2 of 6.148% was used to give the uncertainty in the calculated values.

As the calculated uncertainty in the CASTEP results in Table 4 was unrealistically small, it was decided to plot a much wider range of results by extending the lattice parameters to include Ice Ih, Ice XI, the co-ordinates from the previous CASTEP calculation [5], and to extrapolate the lattice parameters beyond the Ice XI transition to include the variation in lattice parameters represented by the strain broadening in the {131} peak.

Fig. 9 shows the Rietveld goodness-of-fit to the neutron data of the full range of CASTEP energy-minimised structures as well as the historic structures, the "best in class" fit from Table 3 and our CASTEP energy-minimised structure from Table 4, all summarised in Table 6. Each plot has been fitted with a quadratic curve, where the minimum point on the curve represents the best fit to the neutron data, and the shallowness of each quadratic curve demonstrates the relative sensitivity of the Rietveld refinement to each of nine molecular parameters.

The quadratic fit to each of the curves for OH length, HOH angle, wag, rock, pucker and *b*-shift from Fig. 9, were used to generate atomic co-ordinates for this "global minimum" in the goodness-of-fit. From the atomic co-ordinates, the hydrogen bond angles and lengths calculated, and reported in Table 5. The uncertainty and number of significant figures quoted is taken from the difference between this structure and the "best in class" structure in Table 3.

Table 4
Full crystallographic parameters and derived molecular geometry for the CASTEP calculation using the lattice parameters from the "best in class" Rietveld refinement (R_w^2 = 6.111%). The CASTEP calculation was performed with deuterium atoms as for the Rietveld refinement. When tested in the Rietveld refinement, this gave an R_w^2 of 6.148%. Uncertainty in brackets, taken from difference to a CASTEP energy minimisation using similar GSAS lattice parameters within the uncertainty of the Rietveld fit.

	a = 4.4749 Å	b = 7.8452 Å	c = 7.292 Å
O1	0.0	0.659148(2)	0.06178(1)
O2	0.5	0.825815(3)	−0.06178(1)
D1	0.0	0.53731(1)	0.02367(1)
D2	0.0	0.66055(1)	0.19822(1)
D3	0.32228(3)	0.76322(1)	−0.014753(3)
D1O1D2	106.847(5)°	D3O2D3	106.02(2)°
O1D1	0.99543(1) Å	O1D2	0.99496(1) Å
O2D3	0.99561(5) Å		
OD1O = 175.628(1)°	OD2O = 177.135(4)°	OD3O = 177.426(1)°	
D1...O = 1.7724(2) Å	D2...O = 1.7532(1) Å	D3...O = 1.7487(4) Å	
OO1O = 111.475(3)°	OO2O = 109.27(2)°		
Pucker = 0.06179(2)*c*	b-shift = 0.007519(2)*b*	W1 rock = −0.486(1)°	W2 wag = 0.357(3)°

Table 5
Full crystallographic parameters and molecular geometry for the "global minimum" calculated from the quadratic fit to Fig. 9. The atomic co-ordinates have been calculated from the global minimum R_w^2 molecular geometry (HOH, OH, b-shift, pucker, wag and rock) parameters and represent an averaging of the CASTEP and Rietveld results from Fig. 9. The uncertainty and significant figures are the same as for the free Rietveld refinement in Table 3. The fit to the Rietveld refinement was 6.081%.

	a = 4.4749(27) Å	b = 7.8452(5) Å	c = 7.292 Å (fixed)
O1	0.0	0.6567(6)	0.061(8)
O2	0.5	0.8233(3)	−0.061(8)
D1	0.0	0.5392(2)	0.024(4)
D2	0.0	0.6595(1)	0.1977(2)
D3	0.3253(2)	0.7591(1)	−0.0136(2)
D1O1D2	107.5(1)°	D3O2D3	104(2)°
O1D1	0.96(1) Å	O1D2	0.997(2) Å
O2D3	0.992(5) Å		
OD1O = 176.1(1)°	OD2O = 176.9(1)°	OD3O = 175.7(5)°	
D1...O = 1.80(4) Å	D2...O = 1.76(2) Å	D3...O = 1.75(1) Å	
OO1O = 112.0(4)°	OO2O = 109.5(1)°		
Pucker = 0.061(1)*c*	b-shift = 0.010(2)*b*	W1 rock = 0.0°	W2 wag = 0.0°

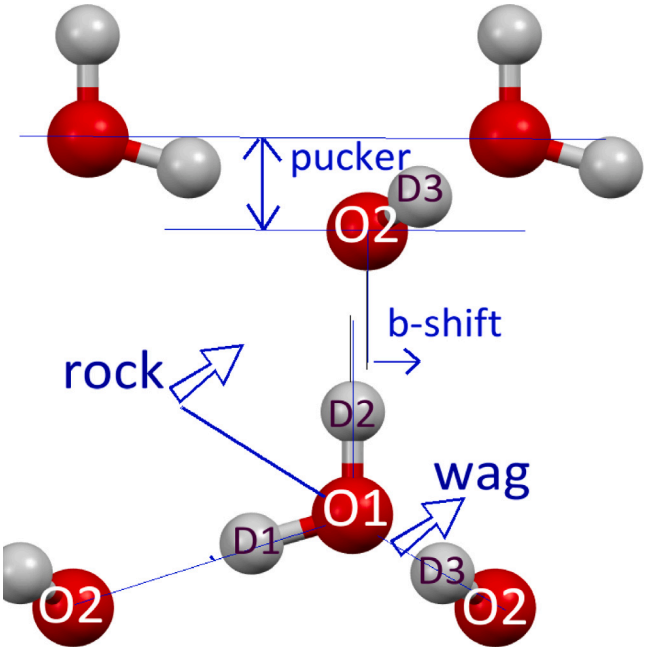

Fig. 8. Diagrammatic representation of molecular geometric parameters for Ice XI when the atomic co-ordinates were freely refined according to "best in class" refinement with Rw = 6.111%.

The final Table 6 summarises the key molecular parameters of these three fits, together with the CASTEP calculations and Rietveld refinements reported by previous workers.

3.3. Plausibility check

The three calculated structures (Rietveld "best in class", CASTEP and the "global minimum" from the quadratic fit to all CASTEP and GSAS structures) can now be compared to the known bond angles and bond lengths in other isomorphs of water as a test of plausibility. For example, the OH bond length in vapour is 0.975 Å and is well outside the range of OH bonds in ice [35], and the HOH bond angle in vapour is 104.5°. Thus, the OH_1 bond lengths of 0.969 Å and 0.96 Å seen in the 'best in class" and "global minimum" refinements (though not the value of 0.995 Å in the CASTEP calculations) are certainly too low. Likewise, the HO_2H bond angle of 104(2)° for the "global minimum" is also too low, as this is the value in water vapour, and the OO_2O bond angle of 108° should act to open up the HO_2H angle.

To attempt to arrive at a plausible structure, a final "plausible" Rietveld refinement was carried out where the O_1H_1 bond length was fixed to the smaller refined value (0.997 Å) of O_1H_3, keeping all other molecular parameters, including the W1 "wag" and W2 "rock", from the "best in class" Rietveld refinement. As reported in Table 7 and summarised in Table 6, this gave the best Rietveld fit of all (R_w^2 = 6.038%), though visually very similar to the "best of class" free Rietveld fit, as seen in the {131} peak in Fig. 10.

Most significantly, Fig. 9 shows that the Rietveld fit parameter R_w^2 is much less sensitive to the value of O_1H_1 than to O_1H_2 and O_2H_3.

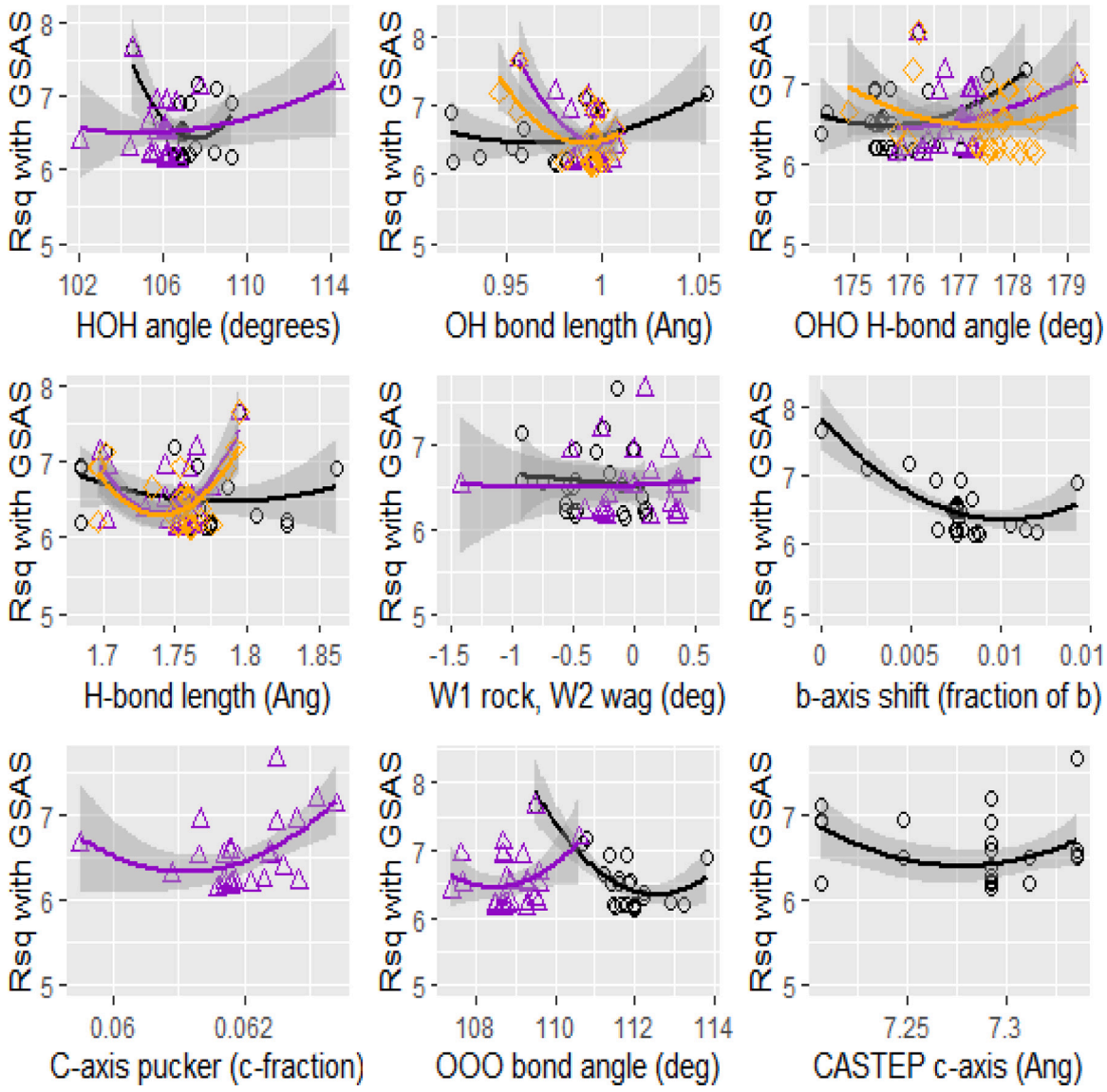

Fig. 9. Plot of Rietveld goodness-of-fit for the full range of molecular parameters for Ice XI, including those generated by DFT calculations. Where values from H1, H2 and H3 are quoted, the colours are in the sequence 1 = black circles, 2 = purple triangles and 3 = orange diamonds.

Table 6
Comparison of Rietveld and CASTEP outputs for HOH bond angles and OH bond lengths.

Method Units	$H_1O_1H_2$ Degrees	$H_3O_2H_4$ Degrees	O_1H_1 Å	O_1H_2 Å	$O_2H_{3/4}$ Å
CASTEP (PW91) [5], energy-minimised lattice	108.5	107.8	0.991	0.993	0.993
CASTEP (PW91) this study R_w^2 = 6.148%	106.8	106.0	0.995	0.995	0.996
Rietveld Leadbetter 1985 [1] R_w^2 = 6.445%	107	114	1.054	0.976	0.946
Rietveld (this study, "best in class") R_w^2 = 6.111%	107.5(6)	106.0(8)	0.969(7)	0.999(6)	0.997(4)
"Global minimum" from Fig. 9; R_w^2 = 6.081%	107.5(1)	104(2)	0.96(1)	0.997(2)	0.992(5)
"Plausible" (Rietveld, OH_1 = OH_3) R_w^2 = 6.038%	107.5(fix)	106.0(fix)	0.997(fix)	0.999(fix)	0.997(fix)

This means that the Rietveld refinement alone is unable to adjudicate on the question of the OH_1 bond length.

To complete this plausibility check, a geometric hydrogen-bond analysis was carried out to evaluate the likely effect of the hydrogen bond forces on the water molecule geometry, and in particular to evaluate whether a shorter OH_1 bond length is physically reasonable.

3.4. Geometric hydrogen-bond analysis of final structure

For ease of conception, for this final section the water molecules are labelled and referred to as HOH, rather than DOD, and using the abbreviation W1 and W2 for HO_1H and HO_2H.

Fig. 11 defines the extracted hydrogen-bond parameters for W1 and W2 as deduced from Table 7.

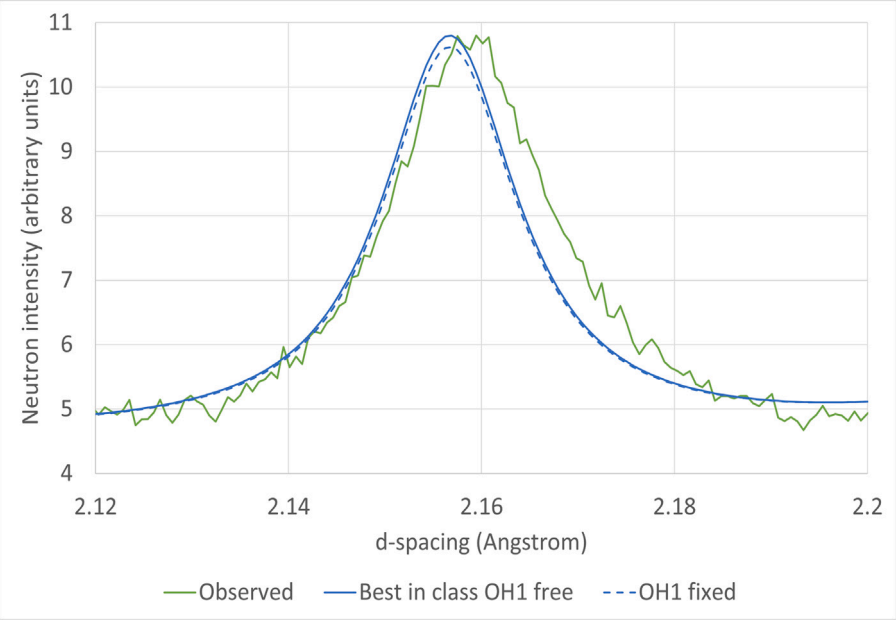

Fig. 10. Neutron diffraction pattern for {131} peak only, showing the "best in class" refinement where the OH_1 bond was refined freely (giving OH_1 = 0.977 Å), compared to the "most plausible" structure from Table 3, where the OH_1 bond length was fixed equal to the OH_3 bond length at 0.997 Å.

Table 7
Full crystallographic parameters and molecular geometry for the recommended "most plausible" crystal structure for Ice XI, obtained from the "best in class" Rietveld free fit but fixing OH_1 to the value of OH_3 (as seen in the CASTEP fit in Table 4). This yielded the lowest R_w^2 of all, being 6.038%.

	a = 4.4749(27) Å	b = 7.8452(5) Å	c = 7.292 Å (fixed)
O1	0.0	0.6578(6)	0.0617(8)
O2	0.5	0.8245(3)	−0.0617(8)
D1	0.0	0.5360(2)	0.0224(4)
D2	0.0	0.6596(1)	0.1986(2)
D3	0.3220(2)	0.7616(4)	−0.0147(2)
D1O1D2	107.5(1)°	D3O2D3	106.0(2)°
O1D1	0.997(1) Å	O1D2	0.999(2) Å
O2D3	0.997(5) Å		
OD1O = 176.4(1)°	OD2O = 176.7(1)°	OD3O = 177.4(5)°	
D1...O = 1.77(4) Å	D2...O = 1.75(2) Å	D3...O = 1.75(1) Å	
OO1O = 111.9(4)°	OO2O = 109.3(1)°		
Pucker = 0.0617(1)	b-shift = 0.0089(2)	W1 rock = −0.096(1)°	W2 wag = −0.25(3)°

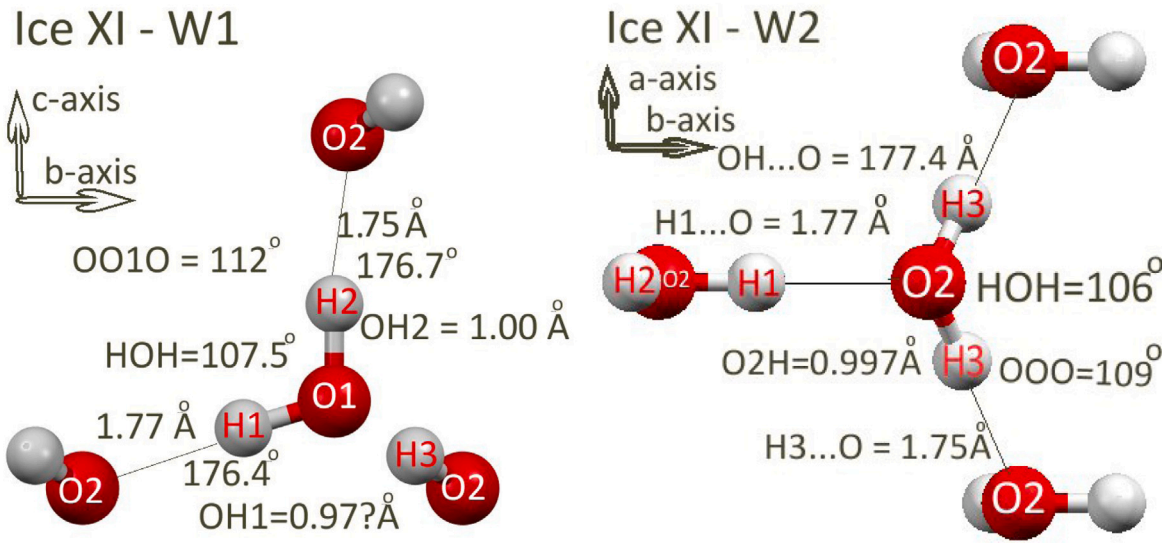

Fig. 11. Graphical summary of plausible Ice XI structure, left: showing W1, viewed down *a*-axis; right: showing W2, viewed down *c*-axis.

The OOO bond angles in Ice XI of 112° and 109° (which in Ice Ih are equal to the tetrahedral angle of 109°) result from the shortening of the *a* lattice parameter and the lengthening of the *b* parameter, together with the b-shift of 0.01*b*. This exerts strain on both water molecules as the HOH bond angle in water vapour is 104.5°. It can be seen that the HO_1H water molecule (W1) has a higher resulting HO1H bond angle (107.5°) than W2 (106°), which is consistent with the higher OO_1O bond angle. Note that W2 has a mirror plane parallel to *b* so is completely symmetric, whereas OH_1 and OH_2 are not symmetrically equivalent. This is also why W2 does not have a "rock" parameter and W1 does not have a "wag" parameter as both would be inconsistent with the symmetry, although of course the dynamic librational modes will all be present.

With regard to the uncertainty in the OH_1 bond length, it can be seen that the H_1...O distance of 1.77 Å is slightly longer than the H_2...O distance of 1.75 Å. This indicates that the OH_1...O hydrogen bond is slightly weaker than the OH_2...O hydrogen bond, and therefore that the OH_1 bond length should be shorter, though not as short as that of water vapour. This therefore argues for an OH_1 bond length that is equal to the smaller of the other two OH angles (0.997 Å), which within the error is equal to the CASTEP value of 0.996 Å (from Table 6). The exact value may be deductible from dynamical measurements, such as from the Raman and neutron inelastic scattering measurements [13].

The similar value (176–177°) of all four OHO hydrogen bond angles is compatible with the small values of "wag" and "rock", showing that both the water molecules have a symmetric orientation with respect to the OOO directions. This together with the values of the HOH bond angles should permit an estimate of the OHO bond stiffness, which is responsible for keeping the Ice Ih structure open and therefore with a lower density than for liquid water, which is needed for life on Earth.

4. Discussion

Overall, it seems there is a good match between the Rietveld refinement from the neutron data and the CASTEP density functional theory measurements. There is also a consistent story in the opening-up of the HOH bond angles in response to the strain from the bent hydrogen bonds OH...O, and it is hoped that this structural study will help in the refinement of simpler hydrogen-bond models for molecular dynamic simulations of water [36].

The main exception is the OH_1 bond length and possibly the HO_2H bond angle. However, Figs. 10 and 9 show that the GSAS-II Rietveld fit is less sensitive to the OH_1 bond length than to other OH bond lengths, and less sensitive to the HO_2H bond angle than to the HO_1H bond angle, but is fairly sensitive to a wide range of other molecular parameters, including the *b*-shift noted by [37]. The physical reason for this is simply crystallographical, and does not reflect what the true bond length of OH_1 (or HO_2H angle) is or should be. Although the Raman spectra have been shown to be insensitive to the OH bond length [20], it is possible that more detailed analysis of the librational spectra [11], using the proposed structure in this study, may resolve this anomaly.

Given the insensitivity of the Rietveld refinement to the O_1H_1 bond length, it is therefore entirely reasonable to take the endorsement of the CASTEP calculations, and propose that the true OH_1 bond length is equal to the smaller of the other two OH bond lengths (Table 7).

The plot of the CASTEP cell *c*-axis in Fig. 9 shows that when squeezing the CASTEP cell according to the Ice XI/Ice Ih phase transition, the optimal value is close to, but slightly lower than the value for the GSAS refined parameters. This may be a scaling effect of the CASTEP simulation.

5. Conclusion

As Ice XI is the only ordered isomorph of Ice Ih, and this is the first study to have refined the atomic co-ordinates of Ice XI freely to result in a plausible structure (as tested with DFT calculations), this study is the first Rietveld refinement giving a detailed and plausible geometry of water due to the self-ordering of water in ice at atmospheric pressure and low temperature. The structure is necessarily strained as it is formed of the ordering of water molecules starting from a disordered Ice 1 h, with the three possible orientations of ordering causing visible anisotropic strain broadening.

The detailed molecular structure of deuterated Ice XI is presented both from Rietveld refinement of neutron diffraction data (Table 3) and Density Functional Theory (Table 4) calculations, with all Cartesian atomic co-ordinates freely refined with no rigid body constraints modelled. The presence of anisotropic lattice strain as evidenced by the {hkl}-dependent line broadening has been modelled in Table 2, the sensitivity of the Rietveld refinement to various molecular parameters has been evaluated in Fig. 9 and the "global minimum" structure derived from the optimised parameters from Fig. 9 is presented in Table 5. As this still gave a physically implausible HO_2H bond angle and O_1H_1 bond length, a final "plausible" model was obtained by reverting to the "best in class " Rietveld free fit but just setting O_1H_1 equal to O_1H_3, as shown in Table 7.

The Rietveld-refined HOH bond angles are 107.5° and 106° for W1 and W2 respectively, which is compatible with the larger strain exerted by the larger OO_1O angle of 112° relative to the OO_2O angle of 109°. The refined HOH bond angles are both intermediate between the tetrahedral angle of 109° and the water-vapour angle of 104.5°, as also shown by our DFT calculations in CASTEP using the Perdew–Wang 1991 functional, and the previous CASTEP study using the same method [5], summarised in Table 6. The OH_1 bond lengths are relatively difficult to deduce, and this is shown to be due to the crystallographic insensitivity of the Rietveld refinement to the OH_1 bond length in particular (Fig. 9). It is possible that the well-studied librational and vibrational spectral modes may shed light on this, although the OH stretching region in the FTIR is known to be insensitive to the OH bond length [13].

The bisectors of the two crystallographically distinct water molecules are at a negligibly small angle to the bisector of the OOO vectors, given as "rock" (for W1) and "wag" (for W2) angles respectively, as defined in Fig. 8. The final structure is presented graphically in Fig. 11.

It is hoped that this study will aid in the development of simpler models for hydrogen-bonding in water, as the balance of forces in this strained structure should enable allocations of hydrogen-bond stiffness in terms of the OH..O hydrogen bond angle and length, as for the Rigid Unit Mode model of silicates [38], or in the allocation of partial charge balancing the known HOH bond stiffness of water [36].

The remaining mystery of the precise value of the OH_1 bond length, together with other anomalies in the neutron spectrum such as the very sharp {062} and {260} peaks (Fig. 6) and the anomalous relative intensities of the {004} peaks (Fig. 3), should keep ice physicists well occupied and retain the mystery of this vital and intriguing molecule.

CRediT authorship contribution statement

Christina M.B. Biggs: Conceptualisation, Methodology, Validation, Formal analysis, Investigation, Writing, Visualisation, Funding acquisition. **Darren L. Oatley-Radcliffe:** Validation, Editing.

Declaration of competing interest

The authors declare that they have no known competing financial interests or personal relationships that could have appeared to influence the work reported in this paper.

Data availability

Data will be made available on request.

Acknowledgements

CMBB acknowledges the sponsorship of the Royal Academy of Engineering, United Kingdom and the Royal Society of Chemistry for a Daphne Jackson Fellowship. CMBB also gratefully acknowledges the help of Dominic Fortes for assisting with the GSAS-II installation and providing the Ice XI neutron diffraction data from [3] data when it proved problematic to recover the [2] data.

CMBB is also grateful for the use of the Supercomputing Wales facility and the helpful input of their support staff.

References

[1] A.J. Leadbetter, R.C. Ward, J.W. Clark, P.A. Tucker, T. Matsuo, H. Suga, The equilibrium low-temperature structure of ice, J. Chem. Phys. 82 (1) (1985) 424–428, http://dx.doi.org/10.1063/1.448763, arXiv:https://pubs.aip.org/aip/jcp/article-pdf/82/1/424/10976867/424_1_online.pdf.

[2] C.M.B. Line, R.W. Whitworth, A high resolution neutron powder diffraction study of D2O ice XI, J. Chem. Phys. 104 (24) (1996) 10008–10013, http://dx.doi.org/10.1063/1.471745, arXiv:https://doi.org/10.1063/1.471745.

[3] A.D. Fortes, Structural manifestation of partial proton ordering and defect mobility in ice ih, Phys. Chem. Chem. Phys. 21 (2019) 8264–8274, http://dx.doi.org/10.1039/C9CP01234F.

[4] C. Knight, S.J. Singer, J.-L. Kuo, T.K. Hirsch, L. Ojamäe, M.L. Klein, Hydrogen bond topology and the ice VII/VIII and ih/XI proton ordering phase transitions, Phys. Rev. E 73 (2006) 056113.

[5] T.K. Hirsch, L. Ojamäe, Quantum-chemical and force-field investigations of ice ih: Computation of proton-ordered structures and prediction of their lattice energies, J. Phys. Chem. B 108 (40) (2004) 15856–15864, http://dx.doi.org/10.1021/jp048434u.

[6] F. Yen, Z. Chi, Proton ordering dynamics of H2O ice, Phys. Chem. Chem. Phys. 17 (2015) 12458–12461, http://dx.doi.org/10.1039/C5CP01529D.

[7] A. Kouchi, Y. Kimura, K. Kitajima, H. Katsuno, H. Hidaka, Y. Oba, M. Tsuge, T. Yamazaki, K. Fujita, T. Hama, Y. Takahashi, S. Nakatsubo, N. Watanabe, UV-induced formation of ice XI observed using an ultra-high vacuum cryogenic transmission electron microscope and its implications for planetary science, Front. Chem. 9 (2021) URL https://www.frontiersin.org/articles/10.3389/fchem.2021.799851.

[8] B.R. Johnson, S.K. Atreya, Feasibility of determining the composition of planetary ices by far infrared observations: Application to martian cloud and surface ices, Icarus 119 (2) (1996) 405–426, http://dx.doi.org/10.1006/icar.1996.0027, URL https://www.sciencedirect.com/science/article/pii/S0019103596900275.

[9] M. Arakawa, H. Kagi, a. Fukazawa, Laboratory measurements of infrared absorption spectra of hydrogen-ordered ice: A step to the exploration of ice XI in space, Astrophys. J. Suppl. Ser. 184 (2009) 361, http://dx.doi.org/10.1088/0067-0049/184/2/361.

[10] M.J. Wójcik, M.G. ug, M. Boczar, L. ukasz Boda, Spectroscopic signature for ferroelectric ice, Chem. Phys. Lett. 612 (2014) 162–166, http://dx.doi.org/10.1016/j.cplett.2014.08.018, URL https://www.sciencedirect.com/science/article/pii/S0009261414006861.

[11] M. Gług, M. Boczar, Ł. Boda, M.J. Wójcik, Analysis of librational modes of ice XI studied by car–parrinello molecular dynamics, Chem. Phys. 459 (2015) 102–111, http://dx.doi.org/10.1016/j.chemphys.2015.08.004, URL https://www.sciencedirect.com/science/article/pii/S0301010415002347.

[12] P. Zhang, Z. Wang, Y.-B. Lu, Z.-W. Ding, The normal modes of lattice vibrations of ice XI, Sci. Rep. 6 (1) (2016) 29273, http://dx.doi.org/10.1038/srep29273.

[13] Y. Liu, L. Ojamäe, Raman and IR spectra of ice ih and ice XI with an assessment of DFT methods, J. Phys. Chem. B 120 (42) (2016) 11043–11051, http://dx.doi.org/10.1021/acs.jpcb.6b07001.

[14] M. Cherubini, L. Monacelli, F. Mauri, The microscopic origin of the anomalous isotopic properties of ice relies on the strong quantum anharmonic regime of atomic vibration, J. Chem. Phys. 155 (18) (2021) 184502, http://dx.doi.org/10.1063/5.0062689, arXiv:https://pubs.aip.org/aip/jcp/article-pdf/doi/10.1063/5.0062689/13564401/184502_1_online.pdf.

[15] M. Schönherr, B. Slater, J. Hutter, J. VandeVondele, Dielectric properties of water ice, the ice ih/XI phase transition, and an assessment of density functional theory, The Journal of Physical Chemistry. B 118 (2014) 590–596.

[16] J.-C. Li, V. Nield, S. Jackson, Spectroscopic measurements of ice XI, Chem. Phys. Lett. 241 (4) (1995) 290–294, http://dx.doi.org/10.1016/0009-2614(95)00660-V, URL https://www.sciencedirect.com/science/article/pii/000926149500660V.

[17] J. Li, Inelastic neutron scattering studies of hydrogen bonding in ices, J. Chem. Phys. 105 (16) (1996) 6733–6755, http://dx.doi.org/10.1063/1.472525, arXiv:https://pubs.aip.org/aip/jcp/article-pdf/105/16/6733/10780408/6733_1_online.pdf.

[18] J. Li, A. Kolesnikov, Neutron spectroscopic investigation of dynamics of water ice, J. Mol. Liq. 100 (1) (2002) 1–39, http://dx.doi.org/10.1016/S0167-7322(02)00009-0, URL https://www.sciencedirect.com/science/article/pii/S0167732202000090.

[19] A. Erba, S. Casassa, R. Dovesi, L. Maschio, C. Pisani, Periodic density functional theory and local-MP2 study of the librational modes of ice XI, J. Chem. Phys. 130 (7) (2009) 074505, http://dx.doi.org/10.1063/1.3076921, arXiv:https://pubs.aip.org/aip/jcp/article-pdf/doi/10.1063/1.3076921/15423692/074505_1_online.pdf.

[20] T. Shigenari, K. Abe, Vibrational modes of hydrogens in the proton ordered phase XI of ice: Raman spectra, J. Chem. Phys. 136 (17) (2012) 174504, http://dx.doi.org/10.1063/1.3702595, arXiv:https://pubs.aip.org/aip/jcp/article-pdf/doi/10.1063/1.3702595/13766426/174504_1_online.pdf.

[21] S.M. Jackson, R.W. Whitworth, Evidence for ferroelectric ordering of ice ih, J. Chem. Phys. 103 (17) (1995) 7647–7648, http://dx.doi.org/10.1063/1.470285, arXiv:https://pubs.aip.org/aip/jcp/article-pdf/103/17/7647/8104894/7647_1_online.pdf.

[22] S.M. Jackson, V.M. Nield, R.W. Whitworth, M. Oguro, C.C. Wilson, Single-crystal neutron diffraction studies of the structure of ice XI, J. Phys. Chem. B 101 (32) (1997) 6142–6145, http://dx.doi.org/10.1021/jp9632551.

[23] A.D. Fortes, Accurate and precise lattice parameters of H_2O and D_2O ice *Ih* between 1.6 and 270 K from high-resolution time-of-flight neutron powder diffraction data, Acta Crystallogr. B 74 (2) (2018) 196–216, http://dx.doi.org/10.1107/S2052520618002159.

[24] B.H. Toby, R.B. Von Dreele, GSAS-II: the genesis of a modern open-source all purpose crystallography software package, J. Appl. Crystallogr. 46 (2) (2013) 544–549, http://dx.doi.org/10.1107/S0021889813003531.

[25] W. Kuhs, M.S. Lehmann, The geometry and orientation of the water molecule in ice ih, J. Physique (1987) http://dx.doi.org/10.1051/jphyscol:1987101.jpa-00226231, URL https://hal.science/jpa-00226231/document.

[26] V.M. Nield, R.W. Whitworth, The structure of ice ih from analysis of single-crystal neutron diffuse scattering, J. Phys.: Condens. Matter 7 (43) (1995) 8259, http://dx.doi.org/10.1088/0953-8984/7/43/006.

[27] R. Howe, R.W. Whitworth, A determination of the crystal structure of ice XI, J. Chem. Phys. 90 (1989) 4450, http://dx.doi.org/10.1063/1.456630.

[28] P.W. Stephens, Phenomenological model of anisotropic peak broadening in powder diffraction, J. Appl. Crystallogr. 32 (2) (1999) 281–289, http://dx.doi.org/10.1107/S0021889898006001, arXiv:https://onlinelibrary.wiley.com/doi/pdf/10.1107/S0021889898006001, URL https://onlinelibrary.wiley.com/doi/abs/10.1107/S0021889898006001.

[29] A.C. Larson, R.B.V. Dreele, General Structure Analysis System (GSAS) manual, Report LAUR 86-748, Report LAUR 86-748 Edition, LosAlamos National Laboratory, 2004, URL https://www.ncnr.nist.gov/xtal/software/gsas.html.

[30] V.F. Petrenko, R.W. Whitworth, Physics of Ice, Oxford University Press, 2002, http://dx.doi.org/10.1093/acprof:oso/9780198518945.001.0001.

[31] S.J. Clark, M.D. Segall, C.J. Pickard, P.J. Hasnip, M.I.J. Probert, K. Refson, M.C. Payne, First principles methods using CASTEP, Z. Kristallogr. - Cryst. Mater. 220 (5–6) (2005) 567–570, http://dx.doi.org/10.1524/zkri.220.5.567.65075.

[32] K. Burke, J.P. Perdew, Y. Wang, Derivation of a generalized gradient approximation: The PW91 density functional, in: J.F. Dobson, G. Vignale, M.P. Das (Eds.), Electronic Density Functional Theory: Recent Progress and New Directions, Springer US, Boston, MA, 1998, pp. 81–111.

[33] D.D. Koelling, B.N. Harmon, A technique for relativistic spin-polarised calculations, J. Phys. C: Solid State Phys. 10 (16) (1977) 3107, http://dx.doi.org/10.1088/0022-3719/10/16/019.

[34] R. Fletcher, Practical Methods of Optimisation, second ed., John Wiley and Sons, New York, 1987.

[35] S. Nanayakkara, Y. Tao, E. Kraka, Capturing individual hydrogen bond strengths in ices via periodic local vibrational mode theory: Beyond the lattice energy picture, J. Chem. Theory Comput. 18 (1) (2022) 562–579, http://dx.doi.org/10.1021/acs.jctc.1c00357.

[36] S.P. Kadaoluwa Pathirannahalage, N. Meftahi, A. Elbourne, A.C.G. Weiss, C.F. McConville, A. Padua, D.A. Winkler, M. Costa Gomes, T.L. Greaves, T.C. Le, Q.A. Besford, A.J. Christofferson, Systematic comparison of the structural and dynamic properties of commonly used water models for molecular dynamics simulations, J. Chem. Inf. Model. 61 (9) (2021) 4521–4536, http://dx.doi.org/10.1021/acs.jcim.1c00794.

[37] S.M. Jackson, R.W. Whitworth, Thermally-stimulated depolarization studies of the ice XI to ice ih phase transition, J. Phys. Chem. B 101 (32) (1997) 6177–6179, http://dx.doi.org/10.1021/jp9632605.

[38] M.T. Dove, Flexibility of network materials and the rigid unit mode model: a personal perspective, Phil. Trans. R. Soc. A 377 (2149) (2019) 20180222, http://dx.doi.org/10.1098/rsta.2018.0222, arXiv:https://royalsocietypublishing.org/doi/pdf/10.1098/rsta.2018.0222, URL https://royalsocietypublishing.org/doi/abs/10.1098/rsta.2018.0222.